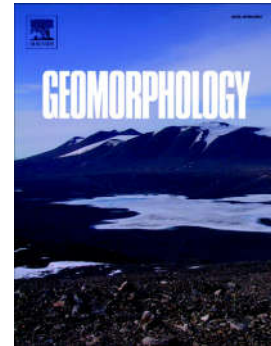


Journal Pre-proof

Incision history of the Mekong River valley revealed by spatially differential exhumation

Ge Yukui, Matthew Fox, Jing Liu-zeng, Huiping Zhang, Xiaoming Shen



PII: S0169-555X(23)00150-2

DOI: <https://doi.org/10.1016/j.geomorph.2023.108730>

Reference: GEOMOR 108730

To appear in: *Geomorphology*

Received date: 23 September 2022

Revised date: 7 May 2023

Accepted date: 8 May 2023

Please cite this article as: G. Yukui, M. Fox, J. Liu-zeng, et al., Incision history of the Mekong River valley revealed by spatially differential exhumation, *Geomorphology* (2023), <https://doi.org/10.1016/j.geomorph.2023.108730>

This is a PDF file of an article that has undergone enhancements after acceptance, such as the addition of a cover page and metadata, and formatting for readability, but it is not yet the definitive version of record. This version will undergo additional copyediting, typesetting and review before it is published in its final form, but we are providing this version to give early visibility of the article. Please note that, during the production process, errors may be discovered which could affect the content, and all legal disclaimers that apply to the journal pertain.

© 2023 Published by Elsevier B.V.

Incision history of the Mekong River valley revealed by spatially differential
exhumation

Yukui, Ge^{1*}, Matthew Fox², Jing Liu-zeng^{3*}, Huiping Zhang¹, Xiaoming Shen⁴

¹*State Key Laboratory of Earthquake Dynamics, Institute of Geology, China Earthquake Administration, Yard No.1, Hua Yan Li, Chaoyang District, 100029, Beijing, China*

²*Department of Earth Sciences, University College London, Gower St., Kings Cross London, WC1E 6BT, UK*

³*School of Earth System Science, Tianjin University, 92 Weijin Rd., Tianjin 300072, China*

⁴*National Institute of Natural Hazards, Ministry of Emergency Management of China, 1 Anningzhuang Rd., Beijing 100085, China*

* Corresponding author: yukuiguo@gmail.com; liu_zeng@tju.edu.cn

Abstract

The evolution of the Mekong River valley offers a singular record of the rock uplift and climate history of southeastern Tibet. Faster erosion rates along the valley than on the flanks caused valley incision and local incision rates may reflect a mix of driving mechanisms, migrating knickpoints linked to a change in base level, and large-scale surface uplift. The thermochronometric-constrained erosion rates in the 2-3 km deep river channel compared to rates outside of the channels provide unique constraints on the driving mechanisms of the river incision. In particular, the onset of river incision at various points along the Mekong River helps identify whether exhumation signals are the result of knickpoint migration which would generate a younger incision upstream, or outgrowth of the plateau, which would produce younger incision downstream. We analyze new and published apatite (U-Th)/He ages collected along two elevation transects in the upper Mekong River: downstream at Tu'Er and upstream at Deqin. The data and thermokinematic modeling predict that the exhumation rates of the valley near Tu Er and Deqin increased more rapidly than those of adjacent high-elevation, low-relief surfaces at ~ 11 Ma and ~ 4 Ma, respectively. Since then, exhumation variations have caused an increase of more than 2 km in the depth of the valley, indicating that the major incision of the Mekong River valley began at ~ 11 Ma near Tu'Er and approximately 4 Ma near Deqin. The results indicate that a major phase of the Mekong River valley incision may have developed and progressed upstream since the Miocene.

1. Introduction

The 4880 km long Mekong River is one of the ten largest rivers globally in terms of water and sediment discharge. Over approximately 3000 km, the Mekong River cuts through narrow valleys 2 to 3 km deep in mountainous regions. The incision of river valleys has played a fundamental role in landscape evolution and sediment transport during the uplift of the Tibetan plateau (e.g., Clift et al., 2006; Zheng et al., 2020). Determining how and when the river valleys of the southeastern Tibetan plateau developed is important to understand the geodynamic mechanisms driving rock uplift and climate change (e.g., Clift et al., 2008; Nie et al., 2018). However, debate continues as to when and how the current bedrock channel of the Mekong River was formed (e.g., Nie et al., 2018; Replumaz et al., 2020; Yuan et al., 2021).

Some of the controversies are due to different definitions of river incision or river formation. To help resolve this debate, it is useful to consider how we judge the formation of a river or river system. Based on the particular research method, there are many different criteria that define the formation of a river. For instance, a source-to-sink detrital provenance approach uses the presence of upstream material being transported to downstream locations as a proxy for the formation of river drainage in the source area. It does not, however, allow for direct reconstruction of the magnitudes nor rate of river incision (e.g., Zheng et al., 2013; Fielding et al., 2018; Schildgen and Beek, 2019). Volcanic flows are valuable geomorphic indicators that may be used to measure river incision (e.g., Pederson et al., 2002), but their ages only place a minimal temporal limit on the period of time during which a valley was carved to the depth at which the flow is preserved (Schildgen and van der Beek, 2019). Rapid exhumation by low-temperature thermochronometric data can be interpreted as an approximation of river incision rates and used to deduce the onset of river formation (e.g., Clark et al., 2005; Flowers and Farley, 2012; Nie et al., 2018; Schildgen et al., 2010). However, river incision is a narrow erosional signal caused by a river or stream in comparison to the surrounding flanks. In general, low-temperature thermochronometric data provide cooling or exhumation information of the rock which the river is incising into (Reiners and Brandon, 2006). This exhumation can

only constrain river incision if differential exhumation between the interfluves on the river valley flanks and the valley bottom can be resolved (e.g., Schildgen et al., 2007; Flowers et al., 2015).

For meaningful quantification, we should first provide a clear definition of river incision, and this definition should be easy to formularize and be tested. We concentrate on the localized river incision and give our definition of the river incision at one point along the length of the river. In a specific localized region, to estimate the timing (t_0) when the current valley started to incise, we require that the average exhumation rate in the river channel (E_r) should be more rapid than that out of the channel (E_b), i.e., an interfluve or low-relief surface outside of the valleys in the southeastern Tibetan plateau; after that time (t_0) the difference of exhumation between the inside and outside of the river channel could result in the current valley (Fig.1). The exhumation information can be inferred by low-temperature thermochronometry, which uses the radioactive decay of a parent nuclide and the accumulation of a corresponding, but leaky, daughter product (Reiners and Brandon, 2006). Different thermochronometric systems are sensitive to different temperatures so that high-temperature systems may record old periods of tectonic activity that may have nothing to do with topographic development. In contrast, lower temperature systems are all less sensitive to previous tectonic events and can constrain topographic development. In particular, the apatite (U-Th)/He thermochronometric system (closure temperature of $\sim 70^\circ\text{C}$) can record relief change as well as exhumation due to its sensitivity to topographically induced temperature fluctuations in the shallow crust (Braun, 2003; Farley, 2002; Reiners and Brandon, 2006). Applying this approach at different positions along the length of the channel allows us to quantify the onset of river incision at different points.

Here, we aim to determine when the current valley of the Mekong River started to form. If the onset of the river incision is simultaneous at different locations, this would support an increase in river discharge and a decrease in river slope along the channel. If the onset becomes younger upstream, this suggests gradual headward knickpoint propagation, consistent with an increase in rock uplift rate. Alternatively, if

the onset becomes younger downstream, this would suggest that the river incision is recording outwards growth of the plateau and local incision. The upper Mekong River flows across relatively low-relief, high-elevation surfaces in the southeastern Tibetan Plateau; hence, the valley of the Mekong River is defined as the elevation difference between the bottom of the valley floor and the adjacent low-relief, high-elevation surfaces (Fig. 2c and 2d). In this study, we focus on the onset of river incision within the upper Mekong River near Tu'er (TE) and Deqin (DQ) (Fig.2) in the southeastern Tibetan Plateau. We use the AHe systems, age-elevation relationship, and inversion via thermal modeling to quantify exhumation rates. Then based on our definition of river incision, we calculate or use nonlinear inverse methods to estimate the onset of the Mekong River incision.

2. Background

The southeastern Tibetan plateau is a region with a complex tectonic and topographic pattern. It experienced large scale shortening, crustal thickening, uplift, transpressional deformation, strike-slip faulting, and tectonic extrusion (Jolivet et al., 2001; Leloup et al., 1995; Tapponnier et al., 2001; Xu and Kamp, 2000; Zhong et al., 1990). The Ailao Shan-Red River strike-slip faults, Langcangjiang faults, Nujiang faults, and the Gaoligong shear zone are all hundreds of kilometer-long continental-scale shear zones with prominent geomorphic expressions in the region (Fig.2b & 3, Burchfiel and Chen, 2013; Jolivet et al., 2001; Liu et al., 2020; Tapponnier et al., 1990; Xu et al., 2015; Zhang et al., 2010; Zhang et al. 2021). These tectonic processes have produced largescale geomorphology characterized by a gradual topographic descent, from 4-5 km to 1-2 km elevation, over ~1000 km across the southeastern Tibetan Plateau. This largescale topographic slope is dissected by continental-scale rivers, such as the Salween, the Mekong, the Yangtze, and the Red Rivers, which carve gorges up to 2-3 kilometers deep across the southeastern Tibetan Plateau region. Between these large valleys, high-elevation and low-relief surfaces can be identified (Clark et al., 2006; Liu-Zeng et al., 2008; Yang et al., 2015). These surfaces are often referred to as relict landscapes (Clark et al., 2006), although this interpretation is still controversial (Yang et al., 2015; Fox et al., 2020), mainly due to

a lack of in situ exhumation constraints across many of the high-elevation, low-relief surfaces (Fox et al. 2020). In this research, we use topographic swath profiles to visualize the configuration of the high-elevation surfaces with respect to the studied river valley (Fig. 2c and 2d).

In the areas near faults and shear zones, the river gorges usually experience enhanced tectonic and/or surface processes compared to other places. This is likely because the rivers are opportunistically cutting down through the more damaged (and therefore weaker) rocks adjacent to the faults and shear zones. Accordingly, rapid exhumation generally occurred along faults, shear zones, and river gorges, which likely reflects a combination of the tectonic activity and river incision in the southeastern Tibetan plateau (Ou et al., 2021; Replumaz et al., 2020; Wang et al., 2018). Furthermore, it can be challenging to attribute inferred high exhumation rates to either active faulting associated within the shear zone or valley incision. Therefore, the comparison of exhumation between different valley bottoms and their surrounding locations is crucial to evaluate whether the low-temperature thermochronometric data reflect localized incision or exhumation of the shear zones (Ge et al., 2020; Henck et al., 2011; Replumaz et al., 2020; Yang et al., 2016). Specifically, the maximum amount of exhumation that can be attributed to fluvial incision is given by the depth of the valley. Where localized exhumation exceeds this limit, this exhumation can be attributed to earlier tectonic activity on the shear zone. Approaches used to constrain exhumation rates have resulted in different conclusions. Yang et al. (2016) reported AHe, AFT, and zircon (U- Th)/He (ZHe) data from the Salween, Mekong, and Yangtze River valley bottoms, which indicates a northward increase in erosion rate, followed by a southward decrease as the distance to the north increases. These data were interpreted with the use of a 3D thermal model and a linearized inversion scheme. The kinematics of the model requires that exhumation rates vary smoothly in space and are very flexible in this way. However, this does not allow researchers to test specific tectonic and landscape evolution scenarios. For example, the approach assumed that the topography remains in a steady state, and thus it is not clear whether these exhumation rates reflect river incision or tectonic activities. Shen et al. (2022) combined

thermochronometric data across the Salween, Mekong, and Yangtze Rivers and interpreted these data with an elegant kinematic model. In this model, rocks travel outwards and over a mantle ramp at a constant rate for 10 million years. The topography stays constant and the shape of the ramp, geothermal gradient, and magnitude of the velocity are determined using a nonlinear inverse model. A combination of model parameters can reproduce the general trends of the data very well using this steady-state model (Shen et al., 2022).

Breaking the study area into different regions with distinct kinematics also helps provide additional resolution on the thermal histories. Ge et al. (2020) compared the variation in exhumation or cooling between the inside and outside of the Gaoligong shear zone to constrain the activity of the shear zones using 3D thermal models. Replumaz et al. (2020) worked to the west of our DQ location and compared the exhumation between the east and west flank of the Mekong valley near Deqing (Fig.2b). The comparison indicates that the tectonic uplift causes differential uplift and exhumation between two flanks of the Mekong valley, uplifting the Kawagebo massif (>6500 m) above the mean plateau elevation (~4800 m). The rapid Quaternary cooling by their model was interpreted as an increased incision in the Mekong valley (Replumaz et al., 2020). In contrast, the rapid exhumation at about 17 Ma recorded by low-temperature thermochronology data is regarded as the onset of river incision by the Mekong River (Nie et al., 2018). Ou et al., (2021) modeled the kinematics of a major fault in the DQ location using a 3D thermo-kinematic approach (Pecube: Braun et al., 2012), which suggests a Quaternary increase of river incision in the Mekong valley. A nonlinear inverse algorithm was used to find a fault history that was consistent with the data. By defining the kinematics in this way, the model is less flexible, and thus the model parameters controlling the fault history are better resolved (Ou et al., 2021). However, there is no way to assess the plausibility of the differences in exhumation rate histories with respect to valley incisions.

Some thermochronometric studies in the southeastern Tibetan Plateau generally show several phases of rapid exhumation (Liu-Zeng et al., 2018; Liu et al., 2021; Shen et al., 2016; Tian et al., 2014; Wang et al., 2012; Wang et al., 2018; Zhang et al., 2022;

Zhang et al., 2016), which have been interpreted as the timing of initial surface uplift, tectonic activity, and/or river incision. Typically, these results are derived from one or more distinct low-temperature thermochronometric profiles and lack spatially comparative exhumation studies between areas with different tectonic or topographic backgrounds. These previous studies highlight that it might be challenging to distinguish between regional exhumation and complex tectonic and topographic changes (England and Molnar, 1990; Schildgen et al., 2018). Here, we provide a specific definition of river valley incision to help address this challenge. We also exploit a simple scenario in which the thermochronometric data is assumed to be the result of a background rock uplift rate with valley incision. We predict thermochronometric data with this scenario with 3D thermal models at different locations along the river to constrain the spatial pattern of the river incision.

3. Analytical methods

3.1. Sampling

To evaluate the exhumation history of the Mekong River valley, we collected five new ages and integrate them with published apatite (U-Th)/He ages from two age-elevation transects near Tu'Er (TE transect), and Deqin (DQ transect) within the upper Mekong River (Fig. 2). Samples of the TE transect were collected along a ~2.5 km high elevation profile at Tu'Er (Fig. 2). The data related to the upper part of this transect were derived from published ages (Ge et al., 2020). Five samples of Jurassic sandstone from the lower part of the TE transect were used for AHe dating (Fig. 1 & 4). Collectively, these existing and new data correspond to an entire transect from the valley floor to the top edge of the river valley, ending near the low-relief surface. The DQ transects, located about 300 km upstream of the Tu'Er transect, span nearly 3 km of elevation from the Mekong valley floor up to the Mekong River bridge (Fig. 2). We compiled all available AHe age data in Figure 4 from the Deqin transect (Liu-Zeng et al., 2018; Replumaz et al., 2020; Yang et al., 2016). Detailed information about the published data is provided in Table S2.

3.2. Apatite (U-Th)/He dating

Apatite concentrates were extracted using standard crushing, sieving, electromagnetic, and heavy liquid mineral separation techniques. Apatite grains with euhedral morphology and no visible inclusions were selected under a microscope, and only grains $> 70 \mu\text{m}$ in both length and width were considered suitable for (U-Th)/He dating. Using digital photographs, grain dimensions were measured to derive the equivalent spherical grain radius and the α -ejection correction factor. Selected single-crystal apatite aliquots per sample were loaded into Nb tubes, degassed by laser heating, and analyzed using ^3He isotope dilution, cryogenic purification, and quadrupole mass spectrometry. Single-grain (U-Th)/He ages of apatite were measured with a Diode and a CO_2 laser heater for He extraction, and a sector ICP-MS for U-Th determinations, at the National Institute of Natural Hazards, Ministry of Emergency Management of China (NINH-MEMC). The age calculation was processed by applying the α -ejection correction factor (F_{α}) (Farley et al., 1996) to each crystal to derive a corrected (U-Th)/He age (Table S1). The age error was calculated based on the analytical uncertainties of the U and Th measurements and the single-grain age variation. Six fragments of Durango apatite were used as reference standards together with and identical to our samples to verify analytical accuracy. A weighted mean average age of $31.7 \pm 0.5 \text{ Ma}$ was obtained for these fragments, which is compatible with the nominal age of the Durango apatite (McDowell et al., 2005).

3.3. Three-dimensional thermo-kinematic modeling

We utilized the 3D thermo-kinematic code Pecube to extract information regarding exhumation, rock uplift, and topography (Braun et al., 2012). This solves the heat equation in 3D and tracks rocks through the evolving thermal field (Braun, 2003; Braun et al., 2012). The thermal histories obtained are used to predict thermochronometric data for comparison with observed data.

The region and sample location of our Pecube models are shown in Fig. 4a and 5a. The new AHe data, as well as the published data from Ge et al. (2020), were used to model the TE transect (Table S2). The regions are characterized by the Mekong River valley and the low-relief surface (Fig. 4a and 5a). For the DQ models, we used all the AHe ages in the Fig. 5a region from Liu-Zeng et al. (2018), Replumaz et al.

(2020), and Yang et al. (2016). We do not consider the ages of the higher temperature systems (AFT and ZHe). This is because these ages reflect earlier phases of exhumation and are not sensitive to valley incision, which is explored in the discussion section. So, instead of attempting to model these complex earlier tectonic processes, we focus solely on the exhumation history after ~20 Ma and use the AHe data alone, as these are most sensitive to relief generation (Fig. 5, e.g., Cuffey et al., 2022; Fox et al., 2017; House et al., 2003; Valla et al., 2011). For the surface boundary conditions of the thermal model, we used the global elevation database GTOPO30 for the modern topography. Topography in the past is scaled by a relief factor. If this factor is set to 1, the paleo-topography is the same as the modern topography. When the factor is set to 0, the paleo-topography is a flat surface tied to the highest point in modern topography. In this way, if the background rock uplift rate remains constant and the relief increases, the erosion rate at the highest point stays constant while the erosion rates in valleys increase. The model thickness is set to 50 km which is comparable to the present crustal thickness in the southeastern Tibetan Plateau (Wang et al., 2010; Li et al., 2006). Table S3 contains the complete thermal and kinetic parameters used in the model.

For both localities, we exploited the Neighborhood Algorithm to quantitatively invert for the unknown model parameters: the basal crustal temperature, the history of rock uplift rate, and landscape evolution over time (relief amplification factor). The investigated time span began at 17 Ma and 20 Ma for the TE and the DQ transects, respectively. We set one-stage of rock uplift based on the inspection of the AHe data and preliminary inverse models. Five variable parameters were explored in each inversion. The detailed list of the explored parameters is given in Table S4. Initial tests of the inversions suggest that TE and DQ models with a one-step tectonic phase and two-step topographic history since the early-middle Miocene are relatively simple and fit the data well (Fig. 6 and S1).

After ~5,000 forward models, both inversion models exhibited stable mean misfit values, and we retrieved the best-fit combination of model parameters. The basal temperature for the DQ inversion does not converge (Fig. S1). Therefore, for

forward modeling, we fixed the basal temperature of the DQ model at $\sim 1000^{\circ}\text{C}$ similar to the TE model.

4. Results and Discussion

For calculating the timing of river incision, using simple conversions of ages to exhumation rates, we provide two simple functions of time and exhumation rate based on our definition of river incision:

$$Er(t_0) > Eb(t_0) \quad (1)$$

$$[Er(t) - Eb(t)] * t_0 + H_0 = H \quad (2)$$

where Er and Eb represent the exhumation rates of the river channel and the area outside of the river channel, respectively. H_0 is the initial elevation difference between the riverbed and interfluvial before the river began to incise. H is the current valley depth (Fig. 1). With these definitions, we can calculate the starting time of river incision (t) based on the exhumation data.

The valley depths at the two locations are similar, ~ 2.5 km near Tu'Er, and ~ 3 km near Deqin, based on our definition of valley depth (Fig. 2). If there are limited tectonic processes to change the elevation difference between the riverbed and the adjacent low-relief, high-elevation surfaces, the depth of the valley is determined by the difference in erosion rate between them (Fig. 7). According to fieldwork and published work (Ge et al., 2020), no recent strong tectonic activity has directly influenced the valley depth near the TE transect. The consistency of the AHe age-elevation relationship also indicates that no tectonic activity disturbs the exhumation of the profile after the early Miocene (Fig. 4b & 5b). Our model result for the TE profile is similar to the results of Ge et al. (2020), except for the transition time. Ge et al. (2020) suggested that the transition time of rapid exhumation was ~ 3 Ma based on the data upper of the TE profile. We supplemented the dataset from the TE profile with additional data from the top to the bottom of the valley, which should provide improved resolution compared to Ge et al. (2020).

Near the Deqin transect, the Kawagarbo massif positioned on the western edge of the Mekong valley is an area of particularly high topography (>6500 m) compared to the surrounding low-relief surface (~ 4800 m), which was considered to be the

result of local tectonic uplift (Ou et al., 2021; Replumaz et al., 2020). We define the valley depth as the relative elevation between the bottom of the valley and adjacent low-relief surfaces on the eastern flank of the Mekong valley that is more consistent with the surrounding, and regional low-relief surface at DQ (Fig. 2d). Ou et al. (2021) proposed the existence of a localized thrust fault along the riverbed of the Mekong River in the Deqin area. However, the consistency of the AHe ages of DQ on both sides of the proposed fault transect suggests that the AHe ages are not sensitive to earlier motion on this fault as Ou et al. (2021) suggested. The valley and the low-relief surface on the eastern flank of the Mekong River are on one side of the specific fault as shown in Fig. 7b. Therefore, we focus on the differences in the exhumation histories of the valley and the low-relief surface on the eastern flank of the Mekong River in this research.

The AHe ages of the TE transect range from ~6.6 to ~15.3 Ma and increase with altitude (Fig. 4). The AHe ages of the DQ transect vary from ~1.3 Ma (sample MK04) at the bottom of the river channel up to ~18.9 Ma (sample DQ11-01) at the top (Fig. 5). The age-elevation relationship of the AHe ages implies ~2 km exhumation between ~15.3 Ma (sample TE11-01) and ~6.6 Ma (sample TE18-4) at the TE transect. Assuming a ~25°C/km geothermal gradient and surface temperatures of ~5-10°C, these valleys have undergone 2-2.5 km exhumation since ~6.6 Ma based on the young AHe age at the bottom of the channel. Comparable to the TE transect, the exhumation was approximately 2-2.5 km after ~1.3 Ma depending on the young AHe age (sample MK04) at the bottom of the channel and the closure depth. The AHe ages collected on the high elevation, low-relief surface are ~15.3 and ~18.9 Ma at the top of the TE transect and DQ transect, respectively. Assuming a ~25°C/km geothermal gradient and surface temperatures of ~5-10°C, the data indicate that the low-relief surface adjacent to the river channels probably eroded ~2-2.5 km (0.1 - 0.2 km/Myr) after ~15.3 and ~18.9 Ma at TE and DQ transects, respectively. More than 2.5 km of exhumation since 10 Ma has occurred on the low-relief surface in the same area as our DQ location. This was confirmed by the model of Ou et al. (2021), which is inconsistent with the hypothesis of the relict surface (Clark et al., 2006). Consequently, the total

exhumation at the TE and DQ valleys would be ~4-6 km, respectively, whereas the adjacent low-relief surface probably underwent ~2-3 km exhumation after the early-middle Miocene. The variation in exhumation magnitudes between the river channel and low-relief surface could have resulted in more than ~2 km of valley incision (or valley depth creation) since the early - middle Miocene, indicating that the current 2-3 km deep valleys were probably built later than early-middle Miocene at both locations. This implies that the old ages (>20 Ma) cannot record information on valley incision. This is why we did not use the older AFT and ZHe ages in our three-dimensional thermo-kinematic inversions. However, these simple calculations do not account for the topography's perturbation of the isotherms, resulting in enhanced geothermal gradients in the valley bottom or transient heat flow due to evolving topography. Therefore, we use the three-dimensional thermo-kinematic code, Pecube, to provide quantitative constraints on the onset of river incision (Braun et al., 2012).

We display Pecube modeling results from our thermo-kinematic inversions on 2D graphs, where the explored parameter space is illustrated and each forward model is colored by its individual misfit value (Fig. 6 and Fig. S1). For both locations, parameter exploration revealed an apparent convergence for the background rock uplift rates of between 0.13 and 0.15 km/Myr since the early-middle Miocene (the medians of boxplots Fig. 6). Before the beginning of river incision, relief was less than ~0.2 times the present-day topographic relief, according to the two inversion models (Fig. S1), which indicates that the depth of the valleys at the DQ and TE sites were less than ~0.6 km.

Regarding the topographic transition, our results indicate that river incision likely began at ~11 Ma at TE and ~4 Ma at DQ (Fig. 6 & 8). Although the river incision commenced at ~11 Ma near TE, the DQ region maintains low exhumation rates between ~18 - ~4 Ma based on the age-elevation relationship and model results (Fig. 4 & 6). The factor that induced river incision near the TE profile at ~11 Ma did not affect the exhumation across the DQ area at that time. This asynchronous incision of the valley near the DQ transect, some ~300 km upstream from the TE transect,

potentially suggests that the upstream propagation of the incision was migrating at a rate of ~ 40 km/Myr. Alternatively, the results may only reflect that lateral migration of the river channel was occurring at both sites at different times. The explanation of lateral migration of the river or local exhumation cannot be ruled out, but upstream migration is more reasonable based on the tendency of low-temperature thermochronometric data along the bottom of the river valley (Yang et al., 2016). The upstream migration rate is consistent with a regional shift in the locus of high erosion between $\sim 26^\circ\text{N}$ and $\sim 28^\circ\text{N}$ in the southeastern Tibetan Plateau region reported by Yang et al. (2016) and Shen et al. (2022). Nevertheless, Yang et al. (2016) proposed that the northwards propagation of the high erosion rates could reflect the northwards advance of the India indenter corner into the Tibetan Plateau. This is based on rate differences between the movement of the locus of high erosion and estimated knickpoint migration. Shen et al. (2022) propose that the crust is flowing southwards along a fixed Moho ramp and is concomitantly exhumed across a steady-state surface. However, the upstream propagation of incision differs from the migration of knickpoints. The movement rate of the locus of high erosion was obtained from data close to the valley bottom (Shen et al., 2022; Yang et al., 2016). The ages and exhumation information of the low-relief interfluvies were not discussed in either of the models. Even though some ages in the interfluvie were employed in the model of Shen et al. (2022), all of the ages (>10 Ma) were artificially reset to 10 Ma because their model only focuses on the events that took place since then. The data from the interfluvies do not exhibit a northwards decrease in age (Fig. 9c) and is therefore dissimilar to the age trend of the bottom of the Mekong River (Shen et al., 2022; Yang et al., 2016). For example, the ages (~ 1 Ma) from the bottom of the DQ profile are young compared to the ages (~ 7 Ma) in the TE profile. However, the AHe ages collected near the high elevation, low-relief surface are ~ 18.9 and ~ 15.3 Ma at the top of the DQ transect and TE transect, respectively. The tendency of the ages along the bottom and the top of the river are inconsistent. If the migration of the locus of high erosion is only concentrated in the river channels, it is unreasonable to explain this as a northwards tectonic advance (Fig. 9b). We propose that the northwards shift of the

locus of high erosion probably reflects river incision and upstream propagation.

Using the stream power model, we can make a first-order estimate of the time required for a knickpoint to propagate through the landscape. The stream power model illustrates how erosion is a product of the upstream drainage area, A , and the local channel slope, S , raised to the powers of m and n respectively, and the erodibility, K , which encompasses bedrock strength, bedload, hydraulic parameters, and climate. Here we use a value of $n=1$ and a value of $m=0.45$ after Yang et al., 2015 and Fox et al., 2020. Therefore, the elevation change at a point along the river channel through time, dz/dt , can be expressed as

$$\frac{dz}{dt} = u - KA^m S^n$$

where u is the rock uplift rate. From this expression, the response time for a knickpoint to travel upstream from a specific x_b to x is given by

$$\tau = \int_{x_b}^x \frac{(x')^n}{KA^m(x')^m} dx'$$

Because K is often unknown, it is common to calculate the normalized response time, χ , which is given by $\chi = \frac{x}{u} K \tau$ (Perron and Royden, 2013). In addition, the slope of the τ -elevation relationship approximates the erosion rate. Therefore, we can quantify the slope of the χ -elevation relationship of the Mekong River at the two locations where we have constrained the river erosion rate. Dividing the local erosion rate by the local slope of the χ -elevation relationship provides an estimate of K . Because we have measured the erosion rate at two locations, we have two estimates of K . These are about $1.3 \text{ m}^{0.1} \text{ Myr}^{-1}$ and $1.8 \text{ m}^{0.1} \text{ Myr}^{-1}$ for the TE and DQ locations, respectively. These values are relatively similar and this provides confidence that this simple relationship between erosion rate and the slope of the χ -elevation relationship is reasonable. Using the average of the two K estimates, we can then convert χ to τ giving the time that it would take a fluvial knickpoint to propagate from TE to DQ (Fig. 10a). This analysis gives a time of approximately 4.4 Ma as shown by the τ values in Fig. 10b and thus an average migration rate of $300 \text{ km}/4.4 \text{ Myr} = 70$

km/Myr. The approach used for the calibration is shown in Fig. 10b. The smooth curve shows the slope of the τ – elevation relationship and the black spots are the measured erosion rates at the corresponding locations. The knickpoint migration rate is similar to the rate resolved by the difference in the timing of the river incision and this provides further confidence in our proposal that the incision is related to knickpoint migration. Differences between the two estimates of migration rate may be due to the assumption of using a fixed drainage area through time, non-linearities in the stream power model, or variable bedrock erodibility along the length of the river.

The formation of high-elevation, low-relief landscapes in the southern Tibetan Plateau remains highly debated (Clark et al., 2006; Fox et al., 2020; Liu-Zeng et al., 2008; Whipple et al., 2017; Willett, 2017; Yang et al., 2015; Yuan et al., 2021; Zhang et al., 2016). The key to resolving this issue lies in the exhumation histories of the high-elevation, low-relief surfaces. The Mekong River bedrock valley experienced 5-6 km of erosion for the TE transect after ~ 15.3 Ma and for the DQ transect after 18.9 Ma, according to AHe ages and model. Provided that the current valley (2-3 km depth) was not an area of elevated topography compared to the surrounding area, the modern interfluvies before the early-middle Miocene and the low-relief, high-elevation surface must have undergone more than 2-3 km exhumation. Our low-temperature thermochronometric data indicate that the high-elevation, low-relief surface near the TE and DQ transects experienced more than ~ 2 km exhumation after the early-middle Miocene. In contrast, some areas of the low-relief surfaces and interfluvies in the southeastern Tibetan Plateau have experienced little erosion during the Cenozoic, inferred from low-temperature thermochronometric age (0.01-0.02 km/Myr, Clark et al., 2005; Clark et al., 2006; Ouimet et al., 2010; Zhang et al., 2016). Thus, the data support the hypothesis that the formation processes of low-relief, high-elevation surfaces are nonuniform across the southeastern Tibetan Plateau based on the large differences in the magnitude of exhumation across different low-relief surfaces. The result does not support the hypothesis of a continuous, homogenous, low-relief surface before the incision of deep valleys. Further in situ exhumation data within the

low-relief landscapes are still required to better constrain the mechanism of the low-relief surface in the southeastern Tibetan Plateau.

5. Conclusion

Exhumation comparisons between different regions can help extract information on tectonic or surface processes. This study provides data to directly constrain the exhumation variation between the Mekong River valley and the adjacent high-elevation, low-relief surface of the southeastern Tibetan Plateau. The difference in exhumation between them causes an increase of ~ 2 km in the depth of valleys after ~ 11 Ma near Tu'Er and after ~ 4 Ma near Deqin, respectively. The results probably suggest that the major river incision of the current Mekong River began near Tu'Er reach at ~ 11 Ma, and progressed upstream to the Deqin reach at ~ 4 Ma. Alternatively, the results probably indicate that lateral migration of the river channel was occurring at both sites at ~ 11 and ~ 4 Ma, respectively. In the southeastern Tibetan Plateau, the exhumation and development of low-relief, high-elevation surfaces are nonuniform. Additional exhumation data are required to more effectively constrain the evolution processes of the Mekong River and the mechanisms of the low-relief surface.

Acknowledgments

This work was supported by the National Nonprofit Fundamental Research Grant of China, Institute of Geology, China, Earthquake Administration (IGCEA2109, IGCEA2003), and National Science Foundation of China (41902213 and 42030305). We thank Wei Wang for help with fieldwork; Heng Wang and Jinyu Zhang for helpful discussion. We express our gratitude to the anonymous reviewers and the editor, Dr. Martin Stokes, for their constructive reviews and invaluable suggestions that have helped to enhance the quality of this manuscript.

References

- Braun, J., 2003. Pecube: a new finite-element code to solve the 3D heat transport equation including the effects of a time-varying, finite amplitude surface topography. *Computers & Geosciences*, 29(6), 787-794.

- Braun, J., van der Beek, P., Valla, P., Robert, X., Herman, F., Glotzbach, C., Pedersen, V., Perry, C., Simon-Labrice, T., Prigent, C., 2012. Quantifying rates of landscape evolution and tectonic processes by thermochronology and numerical modeling of crustal heat transport using PECUBE. *Tectonophysics*, 524, 1-28.
- Burchfiel, B.C., Chen, Z., 2013. Tectonics of the southeastern Tibetan Plateau and its adjacent foreland, 210. Geological Society of America.
- Clark, M.K., House, M.A., Royden, L.H., Whipple, K.X., Burchfiel, B.C., Zhang, X., Tang, W., 2005. Late Cenozoic uplift of southeastern Tibet. *Geology*, 33(6), 525-528.
- Clark, M.K., Royden, L.H., Whipple, K.X., Burchfiel, B.C., Zhang, X., Tang, W., 2006. Use of a regional, relict landscape to measure vertical deformation of the eastern Tibetan Plateau. *J. Geophys. Res.-Earth Surf.*, 111(F3), 23.
- Clift, P.D., 2006. Controls on the erosion of Cenozoic Asia and the flux of clastic sediment to the ocean. *Earth Planet. Sci. Lett.*, 241(3-4), 571-580.
- Clift, P.D., Hodges, K.V., Heslop, D., Hannigan, R., Van Long, H., Calves, G., 2008. Correlation of Himalayan exhumation rates and Asian monsoon intensity. *Nature Geoscience*, 1(12), 875-880.
- Cuffey, K.M., Tripathy-Lang, A., Fox, M., Stock, G.M., Shuster, D.L., Late Cenozoic deepening of Yosemite Valley, USA. *Geological Society of America Bulletin*, 19.
- Deng, Q.D., Zhang, P.Z., Ran, Y.K., Yang, X., Min, W., and Chu, Q.Z., 2003, Basic characteristics of active tectonics of China: Science in China Series D: Earth Science, 46(3), 356-372.
- England, P., Molnar, P., 1990. Surface uplift, uplift of rocks, and exhumation of rocks. *Geology*, 18(12), 1173-1177.
- Farley, K.A., 2002. (U-Th) He dating: Techniques, calibrations, and applications. In: D. Porcelli, C.J. Fallick, R. Wieler (Eds.), *Noble Gases in Geochemistry and Cosmochemistry. Reviews in Mineralogy & Geochemistry*, pp. 819-844.
- Farley, K.A., Wolf, R.A., Silver, L.T., 1996. The effects of long alpha-stopping distances on (U-Th)/He ages. *Geochimica et Cosmochimica Acta*, 60(21), 4223-4229.
- Fielding, L., Najman, Y., Millar, I., Butterworth, P., Garzanti, E., Vezzoli, G., Barfod, D., Kneller, B., 2018. The initiation and evolution of the River Nile. *Earth and Planetary Science Letters*, 489, 166-178.
- Flowers, R.M., Farley, K.A., 2012. Apatite He-4/He-3 and (U-Th)/He Evidence for an Ancient Grand Canyon. *Science*, 338(6114), 1616-1619.
- Flowers, R.M., Farley, K.A., Ketcham, R.A., 2015. A reporting protocol for thermochronologic modeling illustrated with data from the Grand Canyon. *Earth and Planetary Science Letters*, 432, 425-435.
- Fox, M., Carter, A., Dai, J.G., 2020. How Continuous Are the "Relict" Landscapes of Southeastern Tibet? *Front. Earth Sci.*, 8, 15.
- Fox, M., Tripathy-Lang, A., Shuster, D.L., Winn, C., Karlstrom, K., Kelley, S., 2017. Westernmost Grand Canyon incision: Testing thermochronometric resolution.

- Earth and Planetary Science Letters, 474, 248-256.
- Ge, Y., Liu-Zeng, J., Zhang, J., Wang, W., Tian, Y., Fox, M., Zeng, L., Shen, X., Wang, H., Su, Z., Xie, K., 2020. Spatio-temporal variation in rock exhumation linked to large-scale shear zones in the southeastern Tibetan Plateau. *Science China Earth Sciences*, 63(4), 512-532.
- Henck, A.C., Huntington, K.W., Stone, J.O., Montgomery, D.R., Hallet, B., 2011. Spatial controls on erosion in the Three Rivers Region, southeastern Tibet and southwestern China. *Earth Planet. Sci. Lett.*, 303(1), 71-83.
- House, M.A., Wernicke, B.P., Farley, K.A., 1998. Dating topography of the Sierra Nevada, California, using apatite (U-Th)/He ages. *Nature*, 396(6706), 66-69.
- Jolivet, L., Beyssac, O., Goffé, B., Avigad, D., Lepvrier, C., Maluski, H., Thang, T.T., 2001. Oligo-Miocene midcrustal subhorizontal shear zone in Indochina. *Tectonics*, 20(1), 46-57.
- Leloup, P.H., Lacassin, R., Tapponnier, P., Schärer, U., Zhong, D., Liu, X., Zhang, L., Ji, S., Trinh, P.T., 1995. The Ailao Shan-Red River shear zone (Yunnan, China), Tertiary transform boundary of Indochina. *Tectonophysics*, 251(1-4), 3-10.
- Li, S.L., Mooney, W.D., Fan, J.C., 2006. Crustal structure of mainland China from deep seismic sounding data. *Tectonophysics*, 420(1-2), 239-252.
- Liu-Zeng, J., Tapponnier, P., Gaudemer, Y., Ding, L., 2008. Quantifying landscape differences across the Tibetan plateau: Implications for topographic relief evolution. *J. Geophys. Res.-Earth Surf.*, 113(F4), 26.
- Liu-Zeng, J., Zhang, J.Y., McPhillips, D., Reiners, P., Wei, W., Pik, R., Zeng, L.S., Hoke, G., Xie, K.J., Ping, X., Zhong, D.W., Ge, Y.K., 2018. Multiple episodes of fast exhumation since Cretaceous in southeast Tibet, revealed by low-temperature thermochronology. *Earth and Planetary Science Letters*, 490, 62-76.
- Liu, F.B., Danisik, M., Zhong, D.W., Gallagher, K., Nie, J.S., 2021. Distinguishing tectonic versus climatic forcing on landscape evolution: An example from SE Tibetan Plateau. *Geol. Soc. Am. Bull.*, 133(1-2), 233-242.
- Liu, J.L., Chen, X.Y., Tang, Y., Song, Z., Wang, W., 2020. The Ailao Shan-Red River shear zone revisited: Timing and tectonic implications. *Geol. Soc. Am. Bull.*, 132(5-6), 1165-1182.
- McDowell, F.W., McIntosh, W.C., Farley, K.A., 2005. A precise ^{40}Ar - ^{39}Ar reference age for the Durango apatite (U-Th)/He and fission-track dating standard. *Chemical Geology*, 214(3), 249-263.
- Nie, J., Ruetenik, G., Gallagher, K., Hoke, G., Garzione, C.N., Wang, W., Stockli, D., Hu, X., Wang, Z., Wang, Y., Stevens, T., Danišik, M., Liu, S., 2018. Rapid incision of the Mekong River in the middle Miocene linked to monsoonal precipitation. *Nature Geoscience*, 11(12), 944-948.
- Ou, X., Replumaz, A., van der Beek, P., 2021. Contrasting exhumation histories and relief development within the Three Rivers Region (south-east Tibet). *Solid Earth*, 12(3), 563-580.
- Ouimet, W., Whipple, K., Royden, L., Reiners, P., Hodges, K., Pringle, M., 2010. Regional incision of the eastern margin of the Tibetan Plateau. *Lithosphere*,

2(1), 50-63.

- Pederson, J., Karlstrom, K., Sharp, W., McIntosh, W., 2002. Differential incision of the Grand Canyon related to Quaternary faulting - Constraints from U-series and Ar/Ar dating. *Geology*, 30(8), 739-742.
- Perron, J.T., Royden, L., 2013. An integral approach to bedrock river profile analysis. *Earth Surface Processes and Landforms*, 38(6), 570-576.
- Reiners, P.W., Brandon, M.T., 2006. Using thermochronology to understand orogenic erosion, *Annual Review of Earth and Planetary Sciences*. Annual Review of Earth and Planetary Sciences, pp. 419-466.
- Replumaz, A., Jose, M.S., Margirier, A., van der Beek, P., Gautheron, C., Leloup, P.H., Ou, X., Kai, C., Wang, G.C., Zhang, Y.Z., Valla, P.G., Balvay, M., 2020. Tectonic Control on Rapid Late Miocene-Quaternary Incision of the Mekong River Knickzone, Southeast Tibetan Plateau. *Tectonics*, 39(2), 16.
- Schildgen, T.F., Balco, G., Shuster, D.L., 2010. Canyon incision and knickpoint propagation recorded by apatite He-4/He-3 thermochronometry. *Earth and Planetary Science Letters*, 293(3-4), 377-387.
- Schildgen, T.F., Beek, P.A.v.d., 2019. The application of low-temperature thermochronology to the geomorphology of orogenic systems. *Fission-Track Thermochronology and its Application to Geology*, Springer Textbooks in Earth Sciences, Geography and Environment. Springer.
- Schildgen, T.F., Hodges, K.V., Whipple, K.X., Reiners, P.W., Pringle, M.S., 2007. Uplift of the western margin of the Andean plateau revealed from canyon incision history, southern Peru. *Geology*, 35(6), 523-526.
- Schildgen, T.F., van der Beek, P.A., Sinclair, H.D., Thiede, R.C., 2018. Spatial correlation bias in late Cenozoic erosion histories derived from thermochronology. *Nature*, 559(7712), 89.
- Shen, X., Braun, J., Yuan, X., 2022. Southeastern margin of the Tibetan Plateau stopped expanding in the late Miocene. *Earth and Planetary Science Letters*, 583, 117446.
- Shen, X., Tian, Y., Li, D., Qin, S., Vermeesch, P., Schwanethal, J., 2016. Oligocene-Early Miocene river incision near the first bend of the Yangze River: Insights from apatite (U-Th-Sm)/He thermochronology. *Tectonophysics*, 687(Supplement C), 223-231.
- Tapponnier, P., Lacassin, R., Leloup, P., Scharer, U., Dalai, Z., Haisei, W., Ziaohan, L., Shaocheng, J., Lianshang, Z., Jiayou, Z., 1990. The Ailao Shan/Red River metamorphic belt: tertiary left-lateral shear between Indochina and South China. *Nature*, 343(6257), 431-437.
- Tapponnier, P., Zhiqin, X., Roger, F., Meyer, B., Arnaud, N., Wittlinger, G., Jingsui, Y., 2001. Oblique stepwise rise and growth of the Tibet Plateau. *Science*, 294(5547), 1671-1677.
- Taylor, M., and Yin, A., 2009, Active structures of the Himalayan-Tibetan orogen and their relationships to earthquake distribution, contemporary strain field, and Cenozoic volcanism: *Geosphere*, 5(3), 199-214.
- Tian, Y.T., Kohn, B.P., Gleadow, A.J.W., Hu, S.B., 2014. A thermochronological

- perspective on the morphotectonic evolution of the southeastern Tibetan Plateau. *J. Geophys. Res.-Solid Earth*, 119(1), 676-698.
- Valla, P.G., Shuster, D.L., van der Beek, P.A., 2011. Significant increase in relief of the European Alps during mid-Pleistocene glaciations. *Nature Geoscience*, 4(10), 688-692.
- Wang, C.Y., Lou, H., Silver, P.G., Zhu, L., Chang, L., 2010. Crustal structure variation along 30 degrees N in the eastern Tibetan Plateau and its tectonic implications. *Earth Planet. Sci. Lett.*, 289(3-4), 367-376.
- Wang, E., Kirby, E., Furlong, K.P., van Soest, M., Xu, G., Shi, X., Kamp, P.J.J., Hodges, K.V., 2012. Two-phase growth of high topography in eastern Tibet during the Cenozoic. *Nature Geoscience*, 5(9), 640-645.
- Wang, Y., Zhang, P.Z., Schoenbohm, L.M., Zheng, W.J., Zhang, B., Zhang, J.J., Zheng, D.W., Zhou, R.J., Tian, Y.T., 2018. Two-Phase Exhumation Along Major Shear Zones in the SE Tibetan Plateau in the Late Cenozoic. *Tectonics*, 37(8), 2675-2694.
- Whipple, K.X., DiBiase, R.A., Ouimet, W.B., Forte, A.M., 2017. Preservation or piracy: Diagnosing low-relief, high-elevation surface formation mechanisms. *Geology*, 45(1), 91-94.
- Willett, S., 2017. Preservation or piracy: Diagnosing low-relief, high-elevation surface formation mechanisms. *Geology*, 45(8), E421-E421.
- Xu, G.Q., Kamp, P.J.J., 2000. Tectonics and denudation adjacent to the Xianshuihe Fault, eastern Tibetan Plateau: Constraints from fission track thermochronology. *J. Geophys. Res.-Solid Earth*, 105(B8), 19231-19251.
- Xu, Z.Q., Wang, Q., Cai, Z.H., Dong, H.W., Li, H.Q., Chen, X.J., Duan, X.D., Cao, H., Li, J., Burg, J.P., 2015. Kinematics of the Tengchong Terrane in SE Tibet from the late Eocene to early Miocene: Insights from coeval mid-crustal detachments and strike-slip shear zones. *Tectonophysics*, 665, 127-148.
- Yang, R., Fellin, M.G., Herman, F., Willett, S.D., Wang, W., Maden, C., 2016. Spatial and temporal pattern of erosion in the Three Rivers Region, southeastern Tibet. *Earth and Planetary Science Letters*, 433, 10-20.
- Yang, R., Willett, S.D., Goren, L., 2015. In situ low-relief landscape formation as a result of river network disruption. *Nature*, 520(7548), 526.
- Yuan, X.P., Huppert, K.L., Braun, J., Shen, X., Liu-Zeng, J., Guerit, L., Wolf, S.G., Zhang, J.F., Jolivet, M., 2021. Propagating uplift controls on high-elevation, low-relief landscape formation in the southeast Tibetan Plateau. *Geology*.
- Zhang, B., Zhang, J., Zhong, D., 2010. Structure, kinematics and ages of transpression during strain-partitioning in the Chongshan shear zone, western Yunnan, China. *Journal of Structural Geology*, 32(4), 445-463.
- Zhang, G., Tian, Y., Li, R., Shen, X., Zhang, Z., Sun, X., Chen, D., 2022. Progressive tectonic evolution from crustal shortening to mid-lower crustal expansion in the southeast Tibetan Plateau: A synthesis of structural and thermochronological insights. *Earth-Science Reviews*, 226, 103951.
- Zhang, H.P., Oskin, M.E., Liu-Zeng, J., Zhang, P.Z., Reiners, P.W., Xiao, P., 2016. Pulsed exhumation of interior eastern Tibet: Implications for relief generation

mechanisms and the origin of high-elevation planation surfaces. *Earth and Planetary Science Letters*, 449, 176-185.

- Zhang, J.Y., Yang, H.L., Jing, L.Z., Ge, Y.K., Wang, W., Yao, W.Q., Xu, S., 2021. Reconstructing the incision of the Lancang River (Upper Mekong) in southeastern Tibet below its prominent knickzone using fluvial terraces and transient tributary profiles. *Geomorphology*, 376, 21.
- Zheng, H.B., Clift, P.D., He, M.Y., Bian, Z.X., Liu, G.Z., Liu, X.C., Xia, L., Yang, Q., Jourdan, F., 2020. Formation of the First Bend in the late Eocene gave birth to the modern Yangtze River, China. *Geology*, 49(1), 35-39.
- Zheng, H.B., Clift, P.D., Wang, P., Tada, R.J., Jia, J.T., He, M.Y., Jourdan, F., 2013. Pre-Miocene birth of the Yangtze River. *Proceedings of the National Academy of Sciences of the United States of America*, 110(19), 7556-7561.
- Zhong, D., Tapponnier, P., Wu, H.-w., Zhang, L.-S., Ji, S., Zhong, J.-Y., Liu, X.-H., Schärer, U., Lacassin, R., Leloup, F.H., 1990. Large-Scale Strike-Slip-Fault-the Major Structure of Intracontinental Deformation after Collision. *Chinese Science Bulletin*, 35(4), 304-307.

Figures

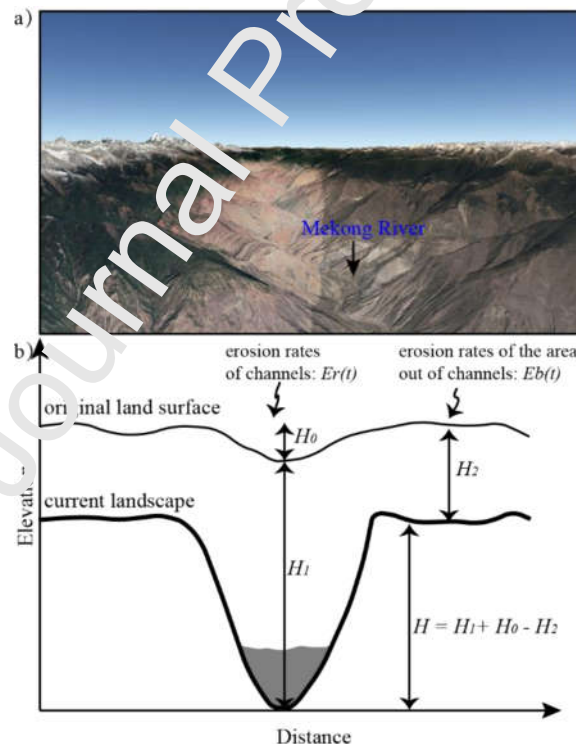


Fig. 1 a) North-facing oblique Google Earth image (Landsat) of the Mekong River, illustrating the contrast between the deeply carved valley and high-elevation low-relief surface. b) Cartoon cross-section of landscape evolution of trunk valleys in the southeastern Tibetan Plateau. During the valley's incision, the low-relief surface

was eroded. When the erosion of the low-relief surface is negligible, the exhumation of the valley represents the increase in valley depth. In several kilometers scale, the isostatic adjustment difference between the channel and the low-relief surface is not taken into account. H : depth of valley; H_0 : depth of valley at t_0 ; H_1 : exhumation of the valley since t_0 ; H_2 : exhumation of paleo-landscape since t_0 . $H > 0$ km means a paleo-valley existed; $H < 0$ km means a positive topography above the current valley at t_0 .

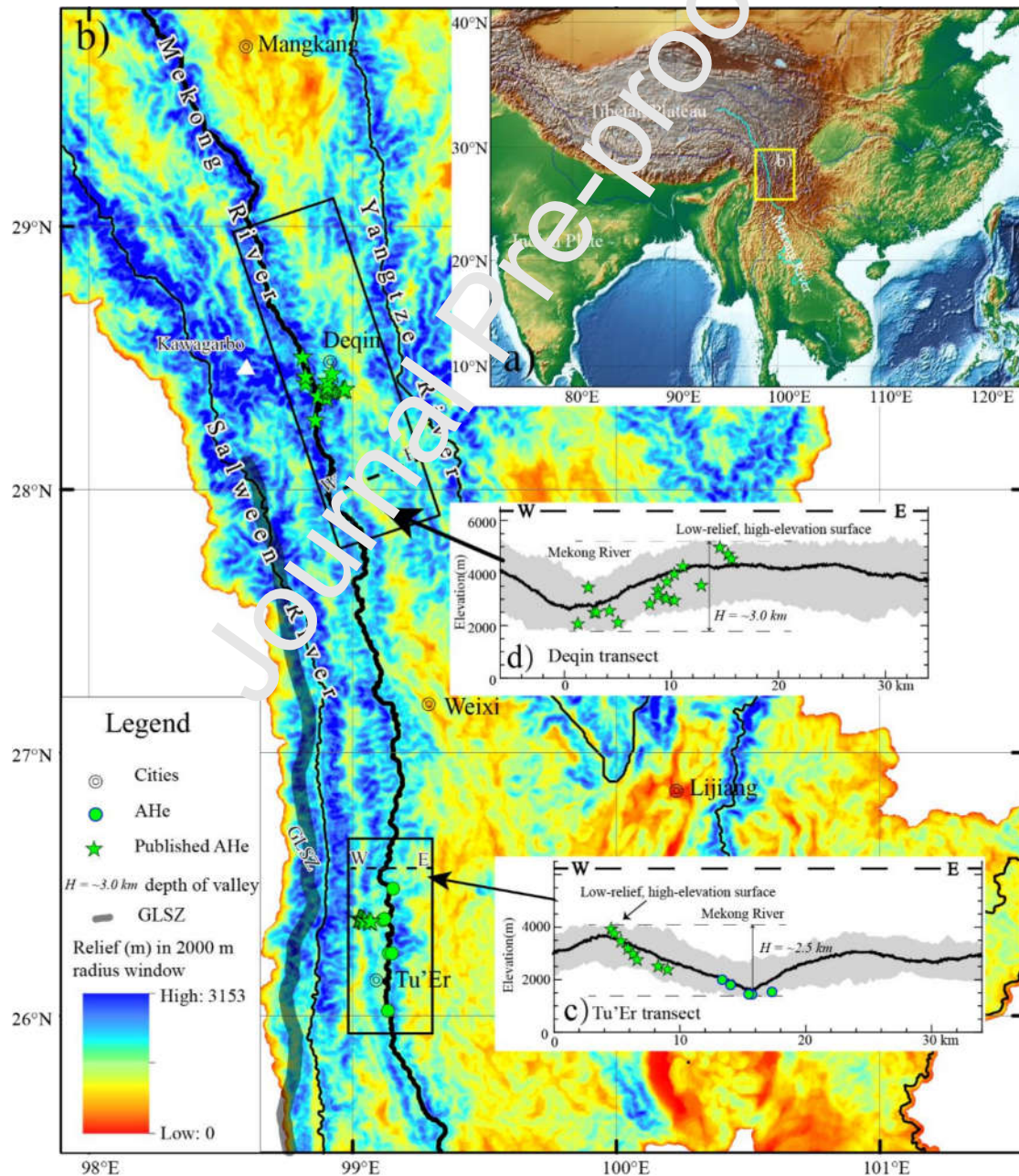


Fig. 2 a) Topography of eastern and southeastern Asia, showing major river in light blue, Mekong drainage basin in blue. GLSZ: Gaoligong shear zone (modified after Tapponnier et al., 2001 and Wang et al., 2018). b) Map of local relief derived from ~90 m digital topography (SRTM DEM, <https://www.gscloud.cn/sources/accessdata/305?pid=302>) calculated over a circular domain (radius = ~ 2km). c) and d) Topographic swath profiles. The swath profiles perpendicular to the Mekong River show the max, min, and average topography, deep incision of the Mekong River, and the projected position of the samples. The circles are the new data; the stars are the data of Ge et al. (2020), Liu-Zeng et al. (2018), Yang et al. (2016), and Replumaz et al. (2020).

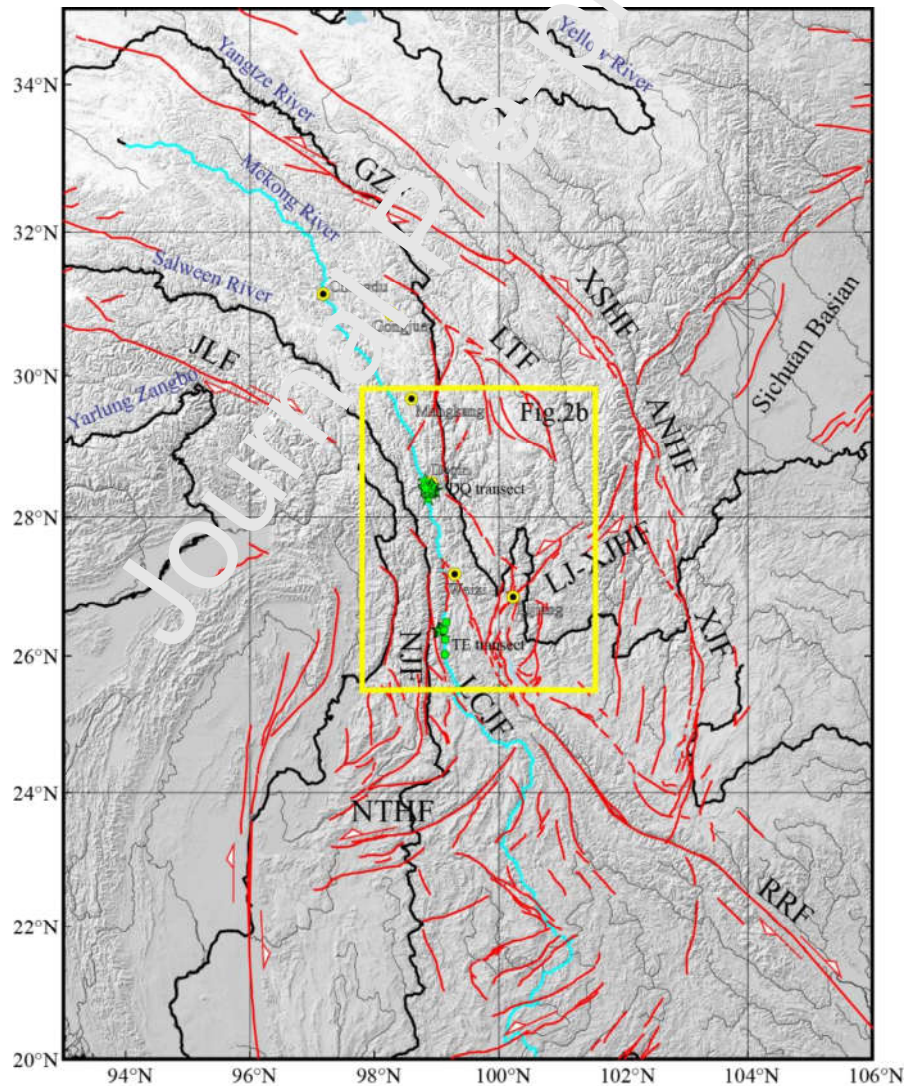


Fig. 3 Topography (SRTM), major rivers, and major structures. Faults are shown by red lines with arrows to indicate the direction of the horizontal motion of the main strike-slip faults, based on the work by Tapponnier et al. (2001), Deng et al. (2003), and Taylor and Yin (2009) and Zhang et al. (2021). GZ-Ganzi Fault; XSHF-Xianshuihe Fault; ANHF-Anninghe Fault; XJF-Xiaojiang Fault; RRF-Red River Fault; LJ-XJHF-Lijiang-Xiaojinhe Fault; LTF-Litang Fault; LCJF-Lancangjiang Fault; NTHF-Nantinghe Fault; NJF-Nujiang Fault; and JLF-Jiali Fault.

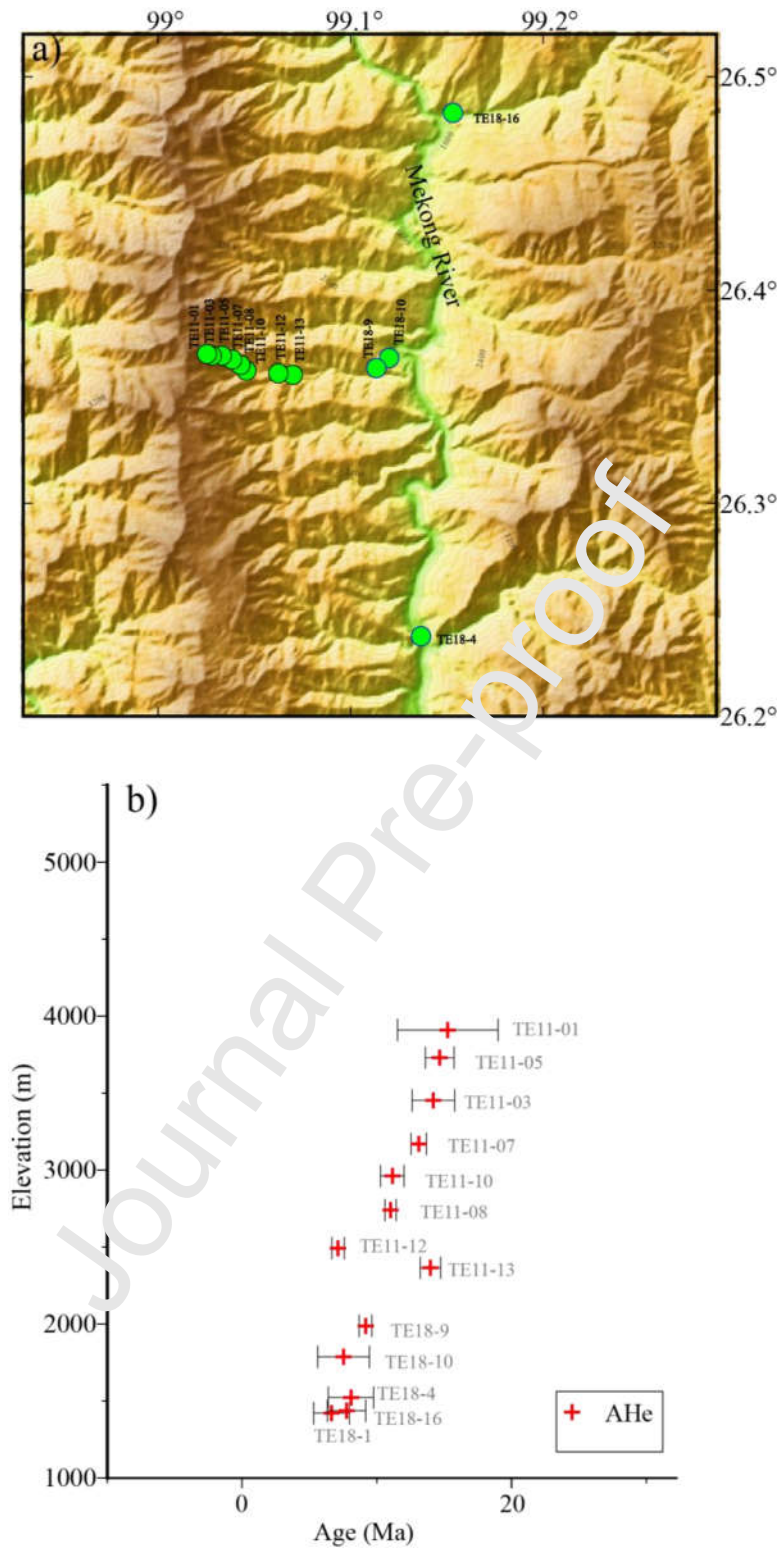


Fig. 4 a) Topography and shaded relief of the TE region and the location of data used in the TE modeling, shown as green circles. b). Age-elevation relationship of the AHe ages of samples shown in panel a). Samples named TE11 are from Ge et al. (2020).

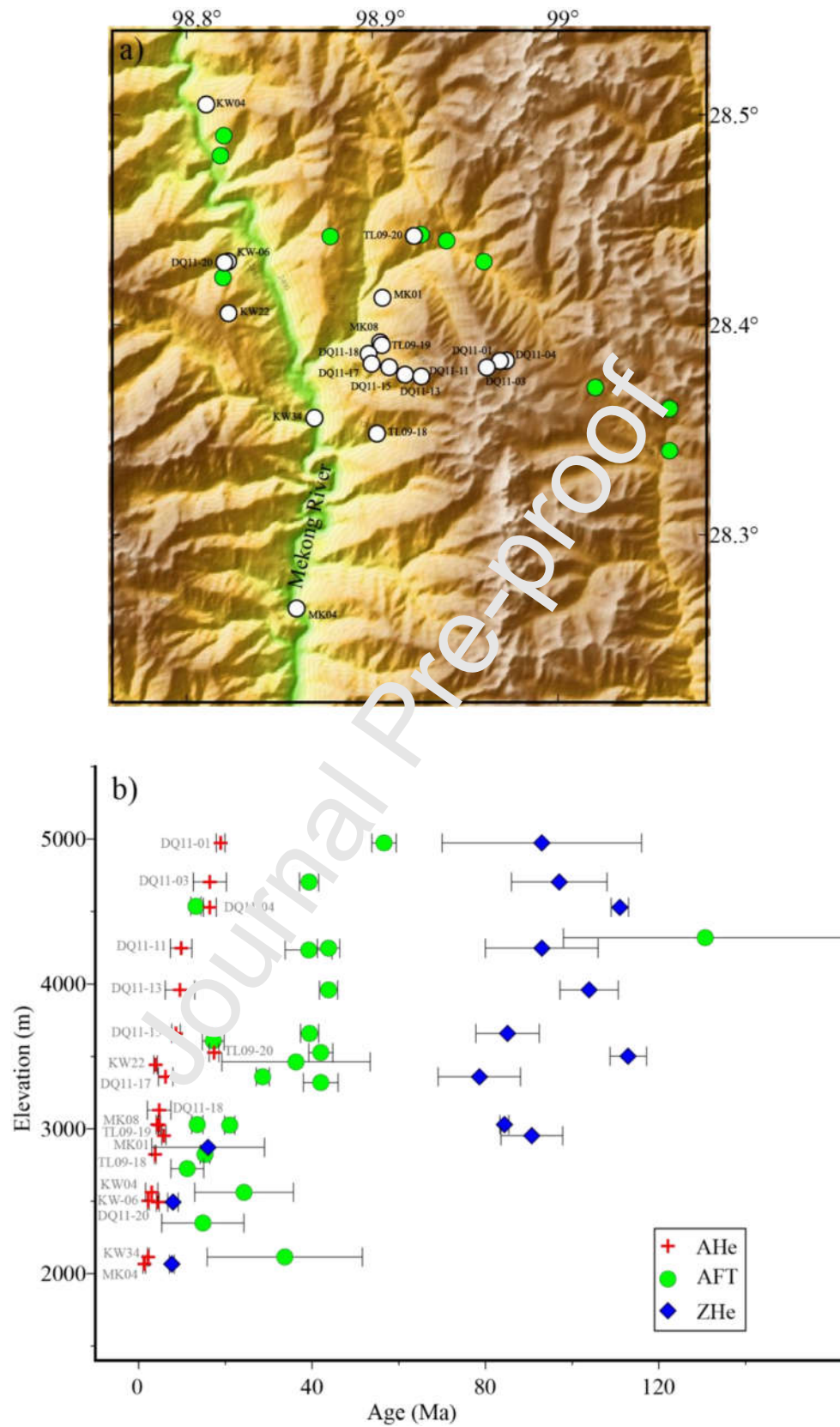


Fig. 5 a) Topography and shaded relief of the DQ region and the location of published data in the DQ region. The circles are the published low-temperature

thermochronology data. White circles with sample numbers are low-temperature thermochronology data with AHe data (nineteen samples) in this region. Green circles are samples with only AFT or/and ZHe data, but no AHe data. b. Age-elevation relationship of all the low-temperature thermochronometric ages of samples shown in panel a). Samples named MK are from Yang et al. (2016); samples named DQ and TL are from Liu-Zeng et al. (2018); samples named KW are from Replumaz et al. (2020).

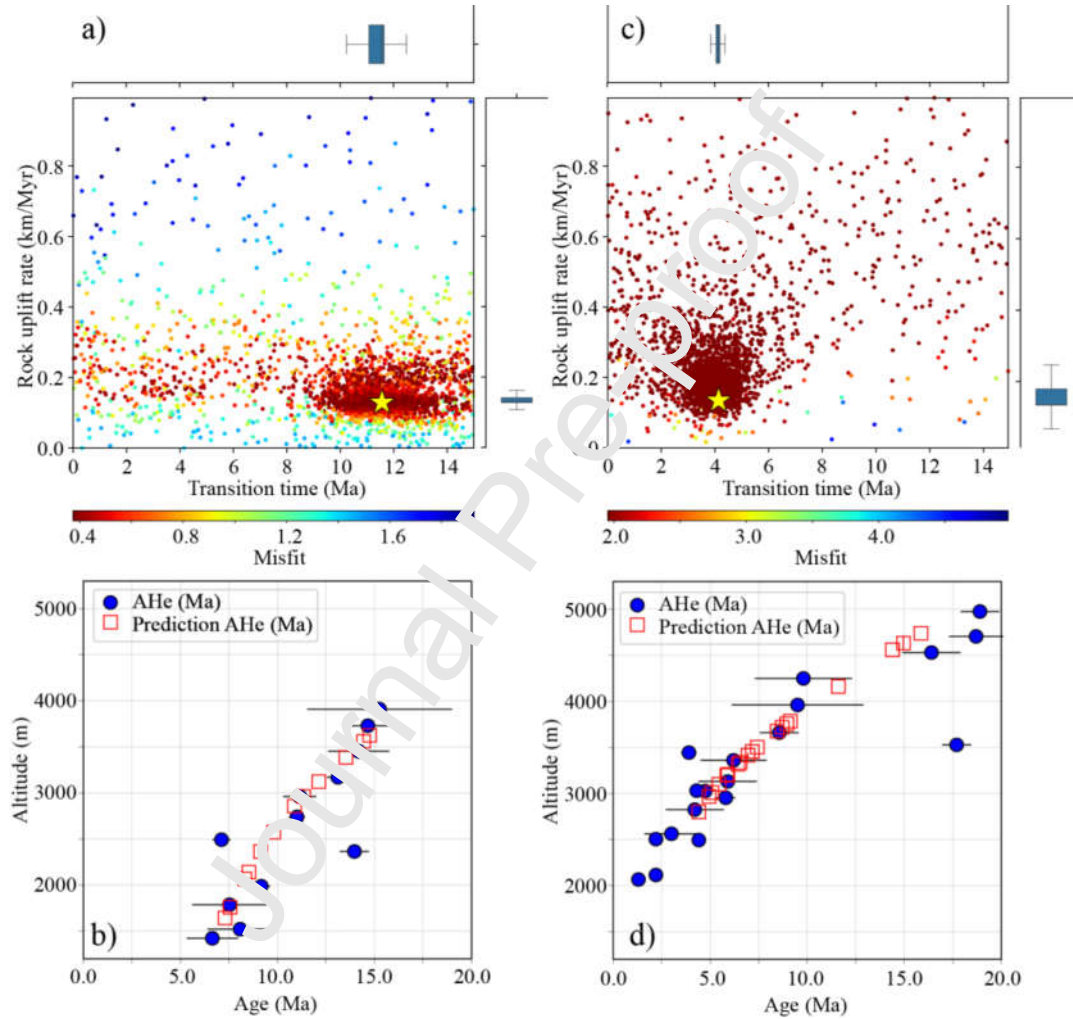


Fig. 6 Pecube inversion results for the TE (a) and DQ transects (c) from 3-D thermokinematic modeling, shown as 2D scatter plots of inversion results and 1D posterior of the box plot. Each point represents an individual forward model, colored by the misfit value. The optimal solution is shown by a star. Transition time: onset of the second topographic phase. A box plot shows the distribution of quantitative data in a way that facilitates comparisons between variables or across levels of a categorical variable. The centerline of the boxplot shows the median, the outer edges

correspond to the lower and upper quartiles, and the whiskers extend to the most extreme observed value within $1.5 \times \text{IQR}$ (interquartile range) from the edges. b) and d) Age elevation profiles of the measured and predicted forward modeling ages of TE transect (b) and DQ transect (d) using Pecube forward 3D thermokinematic model.

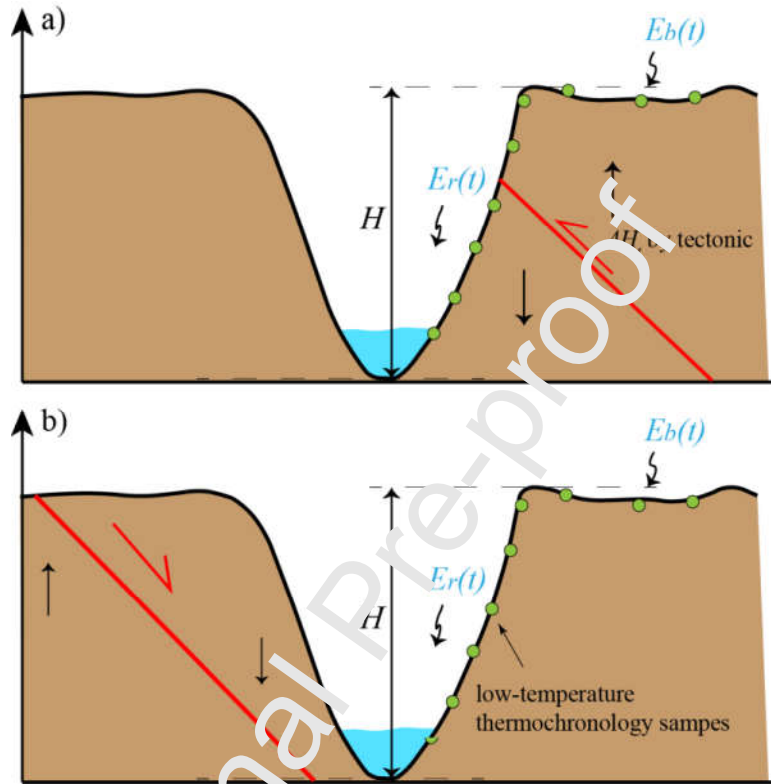


Fig. 7 Relationships of faults, exhumation, and the depth of the valley. Depth of valley H : the relevant elevation between the bottom of the valley and the low-relief surface on the right side of the river. In scenario a), the change of depth of river $\Delta H = [(E_r(t) - E_b(t))t + \Delta H_i]$. ΔH : depth change of the valley, $E_r(t)$: exhumation rates of the valley, $E_b(t)$ exhumation rates of the low-relief surfaces, ΔH_i : the relative change in elevation by tectonics. However, in scenario b) the normal fault would not directly cause the relative change in elevation between the bottom of the river and the low-relief surface on the right flank of the river. $\Delta H = [(E_r(t) - E_b(t))t]$. The change in depth is equal to the difference in exhumation between the two.

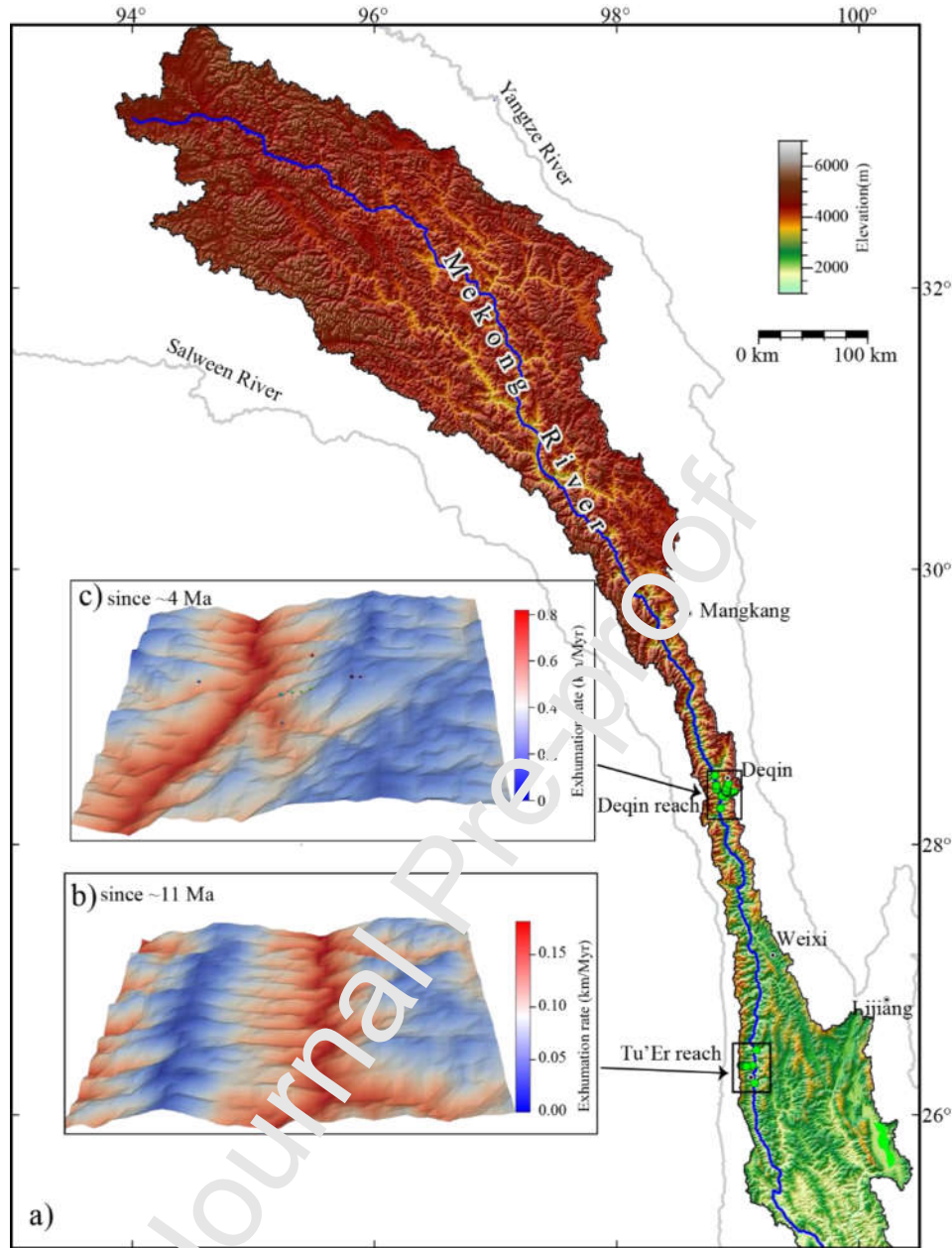


Fig. 8 a) Topography of the upper Mekong drainage basin. Green circles represent the sample location. b) And c) Exhumation rates of valleys and adjacent low-relief surfaces, derived from Pecube inversion and forward modeling, show that the beginning of the primary incision was ~11 Ma at TE and ~4 Ma at DQ, respectively.

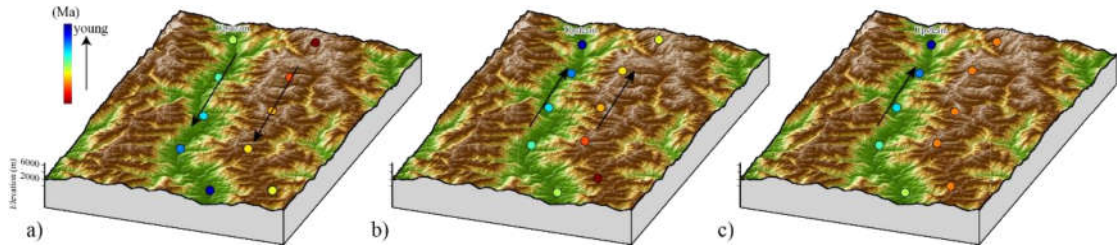


Fig. 9 a) Possible spatial thermochronometric ages pattern for outward propagation model. b) Possible spatial gradients in thermochronometric ages trend along the river and interfluvies under the tectonic advance model and c) under the river migration model.

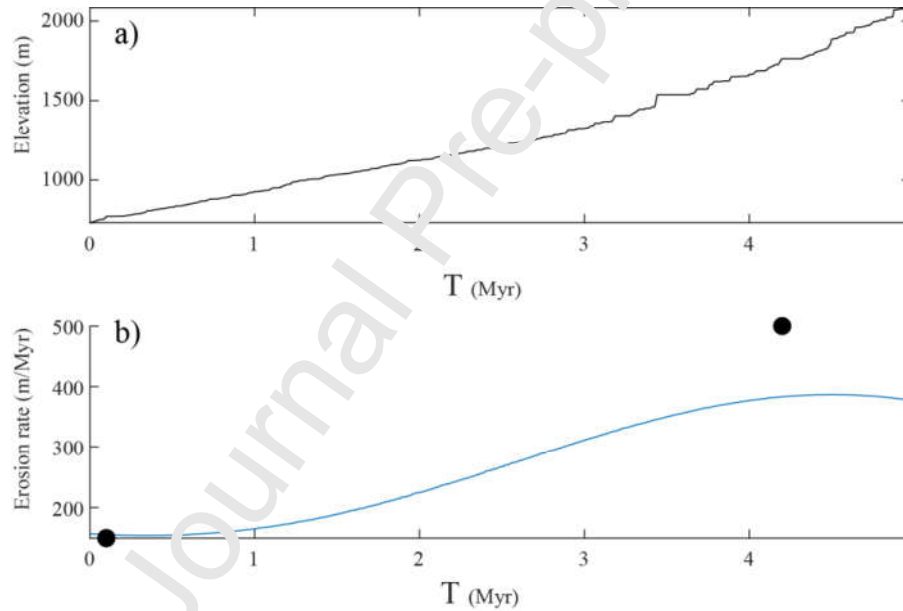


Fig. 10 a) Response time of the Mekong with respect to TE up to the DQ area. The chi values are from Fox et al., 2020 and were calculated with $m=0.45$. b) Calibration for the value of the erodibility requires finding a value of K that leads to the slope of the tau-elevation relationship matching erosion rates. This simplified analysis highlights that the total time required for a wave of incision from TE to DQ is about 5 Ma and that the migration rate would be about 70 km/Myr. The similar trends between the predicted erosion rates and the observed erosion rates support our hypothesis that this incision is related to a wave of incision propagating from downstream.

Declaration of Interest Statement

This manuscript, or any part of it, has not been published and will not be submitted elsewhere for publication while being considered by Geomorphology.

The authors declare that there are no competing financial interests.

Journal Pre-proof

Highlights

Thermochronometric study of the fluvial incision history of the Mekong River.

Presents new and existing apatite (U-Th)/He ages from two elevation transects.

Incision onset at 11 Ma downstream near Tu'Er town and 4 Ma upstream near DeQin town.

2 km deep valley formed by progressive upstream erosion since the Miocene.

Exhumation-development patterns of Tibetan Plateau low-relief surfaces are nonuniform